Remote Pipe Diameter Measurement from a single Image using Laser Scale Projection with a Depth Compensation Model

Alice Weza Fava Bilbáo[1], Leonardo Sales Galvão[1], Daniel Juchem Regner[1], Moacir Wendhausen [1], Gierri Waltrich[1], Carla Alves Marinho Ferreira[2], Tiago Loureiro Figaro da Costa Pinto[1*]

[1] Labmetro, Mechanical Engineering Department, UFSC, 88090470 Florianópolis SC, Brasil - *tiago.pinto@ufsc.br
[2] CENPES/Petrobras, 21941-915, Rio de Janeiro – RJ, Brasil - carlamarinho@petrobras.com.br

Keywords: Optical Metrology, Remote optical inspection, Single-View Measurement, Pipe Diameter, Laser Projection.

Abstract

The dimensional measurement of cylindrical components, such as pipes, is a critical demand for quality control in industrial inspection. Monocular (single-view) computer vision-based approaches offer a low-cost and highly flexible solution but face the fundamental challenge of scale ambiguity. This paper proposes a method for measuring pipe diameter that solves this ambiguity by utilizing the projection of two laser points onto the object from the beam-splitting of a single laser source. The system projects two points with a known and previously calibrated distance onto the object's surface, providing the necessary scale information (mm/pixel) for the image. However, the projection onto the curved surface of the pipe induces a systematic error, as the laser dots land at a different depth (Z) than the depth of the apparent edges of the diameter in the 2D image. The main contribution of this work is the development and validation of a curvature compensation algorithm that mathematically corrects this depth distortion. Experimental results demonstrate that the proposed method, by compensating for the curvature, enables precise diameter measurement with a simple monocular system. For a pipe with a nominal diameter of 165 mm, measured at 6 m distance, the bias in the estimated diameter was reduced from 1.5% to less than 0.2%.

1. Introduction

1.1 Offshore inspection

Monitoring the geometric integrity of risers and pipelines is critical in offshore oil & gas operations. Swell, collapse or torsion often manifest as diametral changes that must be detected safely and efficiently. Historically, this kind of inspection is performed by industrial rope-access climbing, a time-consuming, dangerous and costly operation (Marinho et al., 2012), as seen in Figure 1. More recently, increasing efforts have focused on remote riser inspection using drones, primarily aimed at qualitative assessment through visual analysis. In this context, to extract quantitative data, photogrammetry was evaluated for riser reconstruction in non-prepared scenes (Machado et al., 2021).

Figure 1- Rope-access riser inspection (Buschinelli *et al*., 2020).

State-of-the-art photogrammetry offers accurate inspection but requires a large volume of images, scene preparation, and acquisition network design (Luhmann et al., 2011). Furthermore, in offshore inspection applications, drone operators must be qualified to comply with flight safety procedures and ensure the execution of pre-established trajectories (Salazar et al., 2020), which are essential to provide the adequate scene coverage required for photogrammetric reconstruction.

To overcome the limitations of a qualitative image inspection and the complexity of a complete photogrammetric reconstruction of the scene, we propose a simple, low-cost method to estimate the pipe diameter from a single image by projecting two laser dots of known spacing, building a metric scale directly in the scene and correcting depth differences between the laser projection plane and the silhouette plane of the pipe.

Compared to photogrammetric approaches, which usually require multiple images, careful acquisition planning, and more demanding processing, the proposed method uses a simplified setup that allows diameter estimation from a single image. This reduces data acquisition effort and processing time, making it more suitable for rapid inspection scenarios and potential real-time applications.

Although this work represents the first stage of a study focusing on applications for riser geometry inspections on offshore oil platforms, the present study evaluates the proposed method in laboratory conditions for nominal and calibrated focal lengths, different focal lengths, distances ranging from 2 m to 10 m and four pipe diameters. The results show an improvement from 1.5% error with no depth compensation to less than 0.2% with modelled depth compensation for a 6 m distance.

1.2 Related Works

Currently, photogrammetry is one of the main techniques adopted for image-based industrial inspection, enabling the 3D reconstruction of complex objects and scenes. According to (Luhmann et al., 2011), once an absolute scale is established, it makes it possible to perform high-precision dimensional measurements. Although it is a well-established technique, ensuring accuracy requires the acquisition of multiple images with adequate minimum overlap, as well as complex algorithms as presented in (Triggs et al., 2000). Similarly, the stereo vision technique, according to (Hartley and Zisserman, 2004), also enables precise measurements from 3D reconstruction. However, it requires the use of two rigidly fixed and properly calibrated cameras, and also requires complex algorithms for the determination of corresponding points (Hartley and Sturm, 1997). Laser triangulation also enables measurements of simple part profiles (Muralikrishnan et al., 2012), complex surfaces (Auerswald et al., 2019), distance measurement (Liebe and Coste, 2013), and also of internal duct diameters (Buschinelli et al., 2015). Although these techniques show excellent metrological performance, they present several complexities that often hinder their applicability, such as procedural and constructive complexity, and high computational and financial costs.

In this context, alternative computer vision techniques are suggested, focusing on specific applications. For example, in (Hashemi et al., 2013) a technique is proposed for measuring the cross-sectional diameter deviation of pipes using only a single camera, characterizing a passive monocular system. In (Sun et al., 2014), the measurement of shaft diameters is also performed from a single image, capable of achieving errors on the order of 5.0 µm. As described by (Ayub et al., 2014), a technique is presented for measuring the circularity of cylindrical parts on a production line, in-line, using only a single camera and artificial illumination. Considering a real-time application, (Che and Ratnam, 2018) proposed a low-cost computer vision system method, using a webcam and LED backlighting, to monitor the diameter of parts during the turning process. The method detects the silhouette edges with sub-pixel accuracy and calculates the diameter reduction based on a pre-calibrated scale factor, achieving 0.6% accuracy. In the work of (Arslan, 2018), an analysis of two methods for measuring object distance using a single camera is presented. In the first method, partial calibration is calculated directly from the geometry of Vanishing Points (VP), using the orthocenter, and in the second method, a robust pipeline using statistics, photogrammetry, and vision is used to extract lines, compute VPs, and auto-calibrate.

In the scope of diameter measurement from a single image assisted by structured light projection, (Tan et al., 2021) proposes an in-situ, real-time measurement method for shaft diameters using the projection of a laser line onto the part. It models the measurement using an oblique elliptic cone formed by the laser ellipse on the part and the camera's optical center, achieving a maximum average error of 0.019 mm in tests with the shaft in rotation. In the work of (Li et al., 2024), a method for measuring the diameter of highly reflective shafts is also proposed, using a single camera assisted by laser line projection. The differential of this work is its image processing technique, which fuses a low-exposure image with a high-exposure one to correct the light stripe saturation on reflective surfaces, increasing measurement accuracy by up to six times. In (Wu et al., 2018), a 3D measurement system for the diameter of spheres is proposed, based on the projection of three laser lines. The method's high accuracy is achieved through two main contributions: the use of a neural network (BP) to correct camera distortion and a new algorithm for sub-pixel extraction of the laser line centre. The system reconstructs the 3D points from the detected lines and applies the Least Squares method to fit a sphere equation for subsequent diameter determination.

Considering an application for underwater environments, the work of (Massot-Campos and Oliver-Codina, 2014) presents an underwater 3D reconstruction system that projects a pattern of 25 parallel laser lines using a Diffractive Optical Element (DOE). The technique is based on color channel processing for robust segmentation in high turbidity and on triangulation between the projected light pattern and a single image, generating a non-dense point cloud.

Maintaining the idea of a simplified measurement system with low computational and financial cost and high robustness, this work proposes a technique for measuring the diameter of pipes from a single image, assisted by the projection of two laser points onto the object and featuring depth compensation. The laser points incident on the object are generated from a single laser source, whose light beam is divided by a beam-splitter device, resulting in two points projecting onto the object. The distance between the laser points was previously calibrated and used to insert scale into the scene.

2. Theoretical Background and Proposed Method

2.1 Theoretical Principle

The proposed measurement principle is based on the pinhole camera model. The main distinguishing feature is the consideration of depth difference between the projected laser plane and the silhouette plane of the pipe measured in the image. The geometry of the measurement model is illustrated in Figure 2, which represents a top view of the pipe and the optical system. The following parameters are defined: the observer distance, Z, representing the camera-to-pipe distance; center of projection, C_O; the lens focal length, f; the pipe radius R; the reference length E, defined as half of the distance between the laser dots; and the length, P, which is the distance between the projected blue laser dot on the pipe and the measurement plane.
Furthermore, the model incorporates the distances ν_R and ν_E, which represent the projection of the pipe silhouette, R, and the projection of the laser reference, E, respectively, on the image plane ν. For simplicity purposes the model is derived for the calculation of the radius, R, although in practice it is used for diameter estimation. In this context, the quantities ν_R and ν_E are defined by the distance between the left and right silhouettes of the pipe and the distance between the laser dots, respectively.

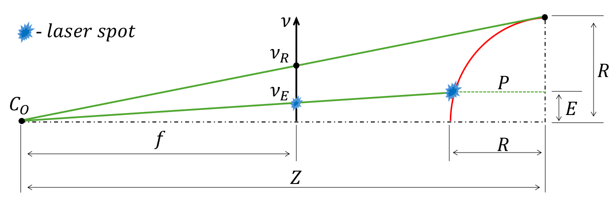

Figure 2. Model for depth compensation.

2.2 Depth Compensation Models (R1, R2, R3)

The first model, $R1$, for diameter calculation adopts a simplified approach, assuming that the laser dot projected onto the part and the silhouette of the measured object lie on the same plane. This approach is mathematically modelled by Equation (1).

$$R1 = \frac{\nu_R . E}{\nu_E} \quad (1)$$

The primary limitation of this simplified model lies in the assumption of a single depth plane for all measured features. In reality, as shown in Figure 2, when a laser is projected onto a cylindrical surface, the incident blue laser dots are located on the frontal part of the pipe, while the silhouettes that define the apparent diameter are located at the widest section of the object.

This depth discrepancy, caused by the pipe's curvature, introduces a systematic underestimation of the true diameter. As the distance between the camera and the object decreases, or the pipe radius increases, the impact of this geometric offset becomes more significant, leading to measurement errors that typically exceed acceptable metrological thresholds for industrial inspection. Consequently, a compensation algorithm is required to account for this difference in depth and restore dimensional accuracy.

To mitigate these systematic errors, model R2 introduces a geometric compensation factor for difference in depth. In this model, the projected dots are considered to be in the pipe front plane, at a distance R from the pipe silhouette plane, as modelled in Equation 2.

$$R2 = \frac{v_R . E}{v_E} . \frac{f}{(v_R - f)} \quad (2)$$

Although model $R2$ improves upon $R1$, it still introduces errors by assuming the laser dots lies exactly on the plane intercepting radius R. This simplification neglects the actual depth variation caused by the pipe's curvature and the laser's lateral displacement.

To address some limitations of previous approaches, model R3 introduces a method that estimates the depth offset as a function of both the pipe radius and the laser's lateral displacement E. By incorporating this relationship into the equations, model R3 aims to reduce geometric bias. Model R3 is defined by Equation (3).

$$R3 = \frac{E . v_R \left(\sqrt{v_E^2 . v_R^2 + v_R^2 . f^2 - v_E^2 . f^2} - f^2 \right)}{v_E^2 . (v_R^2 - f^2)} \quad (3)$$

3. Methodology

3.1 Optical System and Hardware

The measurement system is composed of a Canon EOS80D camera with 24.2 megapixels and a zoom lens with focal length from 24 mm to 135 mm. The projection unit is composed of a dot laser emitter of 450 nm (blue) and 100 mW. For the projection of the two reference points, the periscope accessory, beam divider, from the Renishaw XL-80 interferometer is used, resulting in two parallel beams with 30 mm apart. Figure 3 shows the proposed system and a cropped image example for illustration purposes.

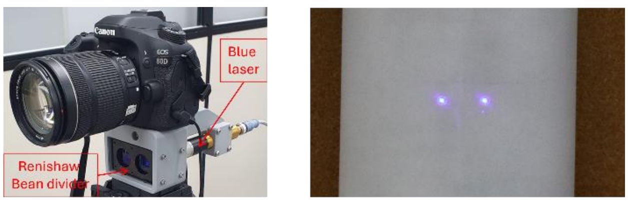

Figure 3. Camera, laser emitter and beam divider mounted on a tripod (left) and an example of acquired image (right).

3.2 Laser dots distance and focal length calibration

To determine the distance, D_L, between the two laser dots emitted by the beam splitter, shown on the right side of Figure 4, a planar object with two circular black targets was used. The center-to-center distance, D_P, of these targets, also illustrated on the right side of Figure 4, was determined through a calibration procedure performed on a Mitutoyo Quick Vision Apex optical coordinate measuring machine, as presented on the left side of the same figure, resulting in a calibrated distance between the target centers of $D_P = (101.195 \pm 0.003)\ mm$.

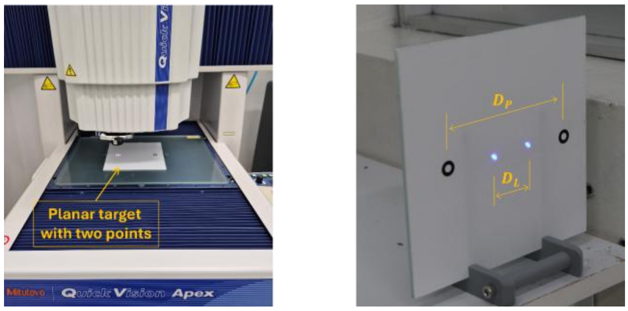

Figure 4. Calibration of the black targets on the planar object using the optical CMM (left). Identification of the center-to-center distances between the mark and the laser dots (right).

Thus, using the distance D_P as a reference, an experiment was conducted to determine the distance D_L. In this procedure, the planar object was positioned at distances ranging from 1 m to 12 m, in steps of 1 m. By image processing the laser dots distance was calibrated to $D_L = (29.646 \pm 0.016)\ mm$.

As the lens focal length is used in the calculation of $R2$ and $R3$, the use of nominal or calibrated focal length may have influence on results quality, although fixed lens and calibration for drone inspection should be avoided in field operations for practical reasons. The measured difference in diameter was negligible (i.e., 0.15 mm) for a pipe with 165 mm diameter, 6 m distance from the camera and nominal focal length of 135 mm and calibrated focal length of 127.04 mm. All subsequent experiments use the EXIF nominal focal length for image processing.

3.3 Experimental Artifacts

For the measurement experiments using the $R1$, $R2$ and $R3$ models, four cylindrical artifacts, pipes, with different nominal diameters and two types of materials were used, as presented in Table 1. Pipe 2, made of aluminium, was coated with a thin layer of white powder to reduce laser beam reflection effects, thereby facilitating the detection of the laser dot center with subpixel resolution.

Artifacts	Pipe 1	Pipe 2	Pipe 3	Pipe 4
Nominal diameter (mm)	100.0	165.0	225.0	300.0
Material	PVC	Aluminium	PVC	PVC

Table 1. Pipes used in diameter measurement experiments.

Figure 5 presents the four artifacts used, with those numbered 1, 2, 3, and 4 shown in Figure 5 (a), (b), (c), and (d), respectively. Among the cylindrical artifacts, only pipe 2, aluminium, was measured using a reference CMM, Mitutoyo model Beyond – A916, with a calibrated diameter value of $(165.061 \pm 0.071)\ mm$.

https://doi.org/10.5194/isprs-archives-XLIX-B2-2026-1133-2026

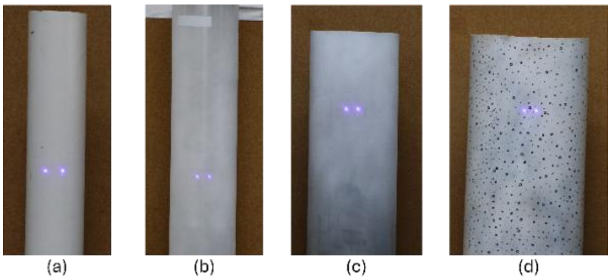

Figure 5. Images of the four cylindrical artifacts, pipes, used in the experiments.

3.4 Experimental Procedure

Two types of experiments were conducted. The first aimed to quantify the measurement error resulting from the effect of varying the lens focal length. In this experiment, only pipe 2 was used. Three sets of measurements were performed by adjusting three different focal lengths: 24 mm for the first set, 50 mm for the second, and 135 mm for the third set. For each focal length set, five repositions and image acquisitions were performed at distances ranging from 1.0 m to 10.0 m, in steps of 1.0 m.
The second experiment consisted of evaluating the influence of the artifact diameter on the measurement results. For this experiment, the diameters of the four pipes were measured using the three proposed models, $R1$, $R2$ and $R3$. Image acquisitions for each pipe were performed at three distances: 4.0 m, 6.0 m, and 8.0 m. Subsequently, a mean value was calculated, and the bias and associated standard deviation were determined, represented by the Type A uncertainty considering a coverage factor of 1 sigma.

3.5 Computational Procedure for Diameter Estimation

To calculate the diameter for the models, software was developed in LabVIEW 2025 Q1. The first step is to measure the pipe diameter ($2 \times VR$) by finding subpixel edges along parallel lines within a user-defined region, based on the mean distance between the detected points on one side and a fitted line to the points on the opposite side. The same ROI is used to measure the distance between the laser dots subpixel centroids ($2 \times VE$), Figure 6 shows the processed image for each step. Edge detection was performed using the IMAQ Rake function (NI Vision Development Module), which estimates edge positions along multiple parallel profiles within a defined region. Subpixel localization was achieved using cubic spline interpolation, with a subpixel resolution of 1/10 pixel. Additionally, subpixel laser dot detection was performed using the centre of mass of the binarized image.

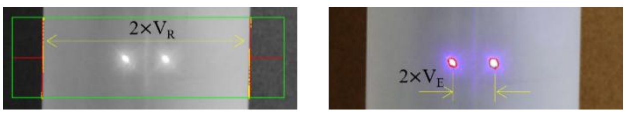

Figure 6. Image processing to detect pipe diameter (left) and laser dots distance (right) (Images cropped).

Regarding contrast, the detection of the laser spots is favoured by the active nature of the system, as the high-intensity laser ensures a high signal-to-noise ratio (SNR), even in low-contrast environments. In contrast, the detection of the pipe silhouette relies on ambient illumination and may be more sensitive to scene and background conditions. Concerning blur, the camera system and pipe was always stationary. Autofocus and shutter speed automatic adjustment was used to mitigate loss of sharpness and contrast, ensuring reliable extraction of both the laser centroid and the pipe silhouette.

4. Experimental Results and Evaluation

4.1 Focal Length and Distance Influence

For all evaluated focal lengths (24, 50, and 135 mm), models R2 and R3 consistently show better results than model R1. For distances between 2 m and 10 m, the mean bias of models R2 and R3 for focal lengths of 135 mm and 50 mm was lower than 0.27 mm, whereas for 24 mm it was 1.25 mm. Model R1 shows a mean bias ranging from 2.9 mm for the 135 mm focal length to 4.10 mm for the 24 mm focal length. The best results were obtained with the 135 mm focal length, which was used in the subsequent analyses.

Using the 135 mm focal length and the calibrated pipe with a nominal diameter of 165 mm, an evaluation was carried out for different distances. Figure 7shows that the simple model R1 exhibits larger errors at shorter distances and consistently higher errors than the proposed models R2 and R3.

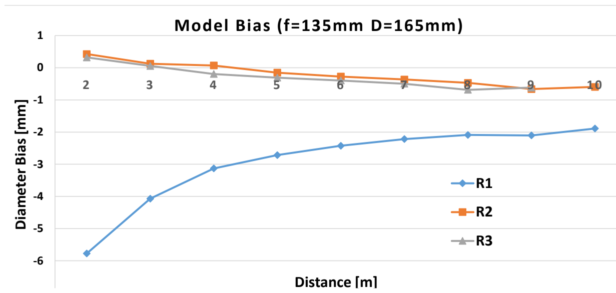

Figure 7. Diameter bias for each model from 2 m to 10 m.

Models R2 and R3 have similar behaviour, while model R1 consistently exhibits the largest errors across all evaluated conditions, highlighting the importance of depth compensation for improving diameter measurement performance. For the 6 m distance the bias for the Model $R1$ is 1.5% of the pipe diameter, whereas Models $R2$ and $R3$ has less than 0.2% bias.

4.2 Influence of Artifact Diameter on Measurement Bias

Figure 8 shows the influence of pipe diameter for each model.

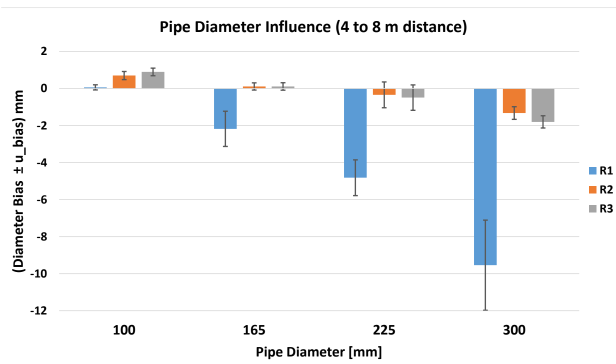

Figure 8. Influence of pipe diameter for each model.

Model R1 exhibits increasing errors as the pipe diameter increases, while maintaining a small error for the smallest tested pipe ($\emptyset\ 100\ mm$). In contrast, the proposed models $R2$ and $R3$ present smaller errors for all other analyzed diameters, demonstrating improved overall performance. Models $R2$ and $R3$ showed similar performance, although $R2$ was marginally better and is the simpler compensation model.

Although the R3 model represents the most complete mathematical formulation, incorporating more parameters than R2, its performance may be influenced by increased uncertainty propagation associated with more complex models. This suggests that the additional rigor of R3 may make it more sensitive to minor noise in the laser spot centroid detection, whereas R2 offers a more balanced trade-off between geometric complexity and experimental robustness. These results are limited to controlled laboratory conditions.

5. Conclusions and Future Perspectives

This work addressed the problem of estimating the pipe diameter from a single image. A simple measurement principle is introduced based on the projection of two laser dots with known spacing. The main contribution lies in modelling and compensating for the depth difference between the laser projection plane and the apparent silhouette of the pipe, which can be a significant source of systematic error in diameter estimation.

Compared to photogrammetric approaches that require multiple images and careful acquisition planning, the proposed method enables diameter estimation from a single image using a simplified setup, reducing both acquisition and processing effort and making it suitable for rapid inspection scenarios and real-time applications.

The experimental results demonstrate that neglecting this geometric effect leads to underestimation of the diameter, particularly at shorter distances and for larger pipes. This behaviour was consistently observed across the evaluated range of pipe diameters (100–300 mm) and distances (2–10 m). For example, for a pipe with nominal diameter of 165 mm measured at 6 m, the bias was reduced from approximately 1.5% to less than 0.2%. Across all evaluated conditions, the compensated models consistently outperformed the approach without depth compensation, confirming that depth correction is necessary for achieving metrological reliability in this context.

From an application perspective, the proposed method offers a simplified alternative to photogrammetry and stereo vision for scenarios where rapid assessment is required. The ability to extract metric information from a single image, with minimal setup and reduced computational demand, makes it particularly attractive for remote inspection tasks, such as offshore riser monitoring using drones. The results obtained at distances up to 10 m indicate that the method is compatible with typical operational constraints of such environments.

At the same time, the present study was conducted under controlled laboratory conditions, and some limitations must be acknowledged. The robustness of the method under varying illumination, surface reflectivity, occlusions, and platform instability still needs to be assessed. In addition, although the uncertainty analysis based only on Type A evaluation provides a consistent estimate of measurement repeatability, a complete uncertainty budget, including Type B contributions, remains to be established for field deployment.

Future work will focus on bridging the gap between laboratory validation and real-world operation. This includes the integration of the system into a drone platform and the evaluation of performance under dynamic conditions. In the laboratory experiments, the laser was manually centred on the pipe for each acquisition; however, potential misalignment may influence the measurement results, particularly under dynamic conditions. This effect was not evaluated in the present study and will be addressed in future work. The automation of region-of-interest detection using learning-based approaches is also expected to play a key role in enabling fully autonomous measurements. Furthermore, tests with a wider range of materials, surface and background conditions will be necessary to consolidate the method's applicability in practical inspection scenarios.

In summary, this study shows that accurate diameter measurement from a single image is feasible when the underlying geometry is properly modelled. By combining a simple optical setup with an appropriate depth compensation strategy, it is possible to achieve a level of accuracy that approaches more complex systems, while preserving operational simplicity. This balance between simplicity and performance is what ultimately supports the potential of the proposed approach for real inspection applications.

References

Arslan, O., 2018. Accuracy assessment of single viewing techniques for metric measurements on single images. IET Comput. Vis. 12, 693–701. https://doi.org/10.1049/iet-cvi.2017.0549

Auerswald, M.M., von Freyberg, A., Fischer, A., 2019. Laser line triangulation for fast 3D measurements on large gears. Int. J. Adv. Manuf. Technol. 100, 2423–2433. https://doi.org/10.1007/s00170-018-2636-z

Ayub, M.A., Mohamed, A.B., Esa, A.H., 2014. In-line Inspection of Roundness Using Machine Vision. Procedia Technol. 15, 807–816. https://doi.org/10.1016/j.protcy.2014.09.054

Buschinelli, P., Pinto, T., Silva, F., Santos, J., Albertazzi, A., 2015. Laser Triangulation Profilometer for Inner Surface Inspection of 100 millimeters (4″) Nominal Diameter. J. Phys. Conf. Ser. 648. https://doi.org/10.1088/1742-6596/648/1/012010

Buschinelli, P., Salazar, J.D., Regner, D., Oliveira, D., Machado, M., Marcellino, G., Sales, D.C., Santos, J.M., Marinho, C.A., Stemmer, M.R., Pinto, T.C., 2020. Targetless photogrammetry network simulation for inspection planning in oil and gas industry. ISPRS Ann. Photogramm. Remote Sens. Spat. Inf. Sci. V-1–2020, 285–291. https://doi.org/10.5194/isprs-annals-V-1-2020-285-2020

Che, J.K., Ratnam, M.M., 2018. Real-time monitoring of workpiece diameter during turning by vision method. Measurement 126, 369–377. https://doi.org/10.1016/j.measurement.2018.05.089

Hartley, R., Zisserman, A., 2004. Multiple View Geometry in Computer Vision, Second Edi. ed. Cambridge University Press, Cambridge.

Hartley, R.I., Sturm, P., 1997. Triangulation. Comput. Vis. Image Underst. 68, 146–157. https://doi.org/10.1006/cviu.1997.0547

Hashemi, S.H., Moradpour, M.A., Karimi, E., Kazemi, M., 2013.

The use of machine vision inspection for out of roundness measurement in steel pipes. First Iran. Conf. Pattern Recognit. Image Anal. PRIA 2013 1–5. https://doi.org/10.1109/PRIA.2013.6528453

Li, C., Xu, X., Liu, S., Ren, Z., 2024. A Method for Measuring Shaft Diameter Based on Light Stripe Image Enhancement. Sensors 24. https://doi.org/10.3390/s24010303

Liebe, C.C., Coste, K., 2013. Distance measurement utilizing image-based triangulation. IEEE Sens. J. 13, 234–244. https://doi.org/10.1109/JSEN.2012.2212428

Luhmann, T., Robson, S., Kyle, S., Harley, I., 2011. Close Range Photogrammetry, First Edit. ed. Whittles Publishing.

Machado, M., Marcellino, G., Salazar, J.D., Regner, D.J., Buschinelli, P., Santos, J.M., Marinho, C., Pinto, T.C., 2021. RPA positioning error influence on close range photogrammetry for industrial inspection. Int. Arch. Photogramm. Remote Sens. Spat. Inf. Sci. - ISPRS Arch. 43, 541–548. https://doi.org/10.5194/isprs-archives-XLIII-B2-2021-541-2021

Marinho, C.A., Souza, C. De, Motomura, T., Silva, A.G. da S., 2012. In-service flares inspection by unmanned aerial vehicles (UAVs). 18th World Conf. Nondestruct. Test. 16–20.

Massot-Campos, M., Oliver-Codina, G., 2014. Underwater laser-based structured light system for one-shot 3D reconstruction. Proc. IEEE Sensors 2014-Decem, 1138–1141. https://doi.org/10.1109/ICSENS.2014.6985208

Muralikrishnan, B., Ren, W., Everett, D., Stanfield, E., Doiron, T., 2012. Performance evaluation experiments on a laser spot triangulation probe. Meas. J. Int. Meas. Confed. 45, 333–343. https://doi.org/10.1016/j.measurement.2011.11.012

Salazar, J.D., Buschinelli, P., Marcellino, G., Machado, M., Rodrigues, H., Regner, D., Oliveira, D., Santos, J.M., Marinho, C.A., Stemmer, M.R., Pinto, T.C., 2020. 3D PHOTOGRAMMETRIC INSPECTION of RISERS USING RPAS and DEEP LEARNING in OIL and GAS OFFSHORE PLATFORMS. Int. Arch. Photogramm. Remote Sens. Spat. Inf. Sci. - ISPRS Arch. 43, 1265–1272. https://doi.org/10.5194/isprs-archives-XLIII-B2-2020-1265-2020

Sun, Q., Hou, Y., Tan, Q., Li, C., 2014. Shaft diameter measurement using a digital image. Opt. Lasers Eng. 55, 183–188. https://doi.org/10.1016/j.optlaseng.2013.11.005

Tan, Q., Kou, Y., Miao, J., Liu, S., Chai, B., 2021. A model of diameter measurement based on the machine vision. Symmetry (Basel). 13, 1–15. https://doi.org/10.3390/sym13020187

Triggs, Bill, Mclauchlan, P., Hartley, R., Fitzgibbon, A., 2000. Bundle Adjustment – A Modern Synthesis, in: Triggs, B. (Ed.), Vision Algorithms: Theory and Practice; Vol. 1883. Springer-Verlag, Corfu, Greece, pp. 298–372.

Wu, F., Mao, J., Zhou, Y. feng, Qing, L., 2018. Three-line structured light measurement system and its application in ball diameter measurement. Optik (Stuttg). 157, 222–229. https://doi.org/10.1016/j.ijleo.2017.11.068